Temperature Distribution During ICG-Dye-Enhanced Laser Photocoagulation of Feeder Vessels in Treatment of AMD-Related Choroidal Neovascularization

Liang Zhu[1]
Department of Mechanical Engineering,
University of Maryland,
Baltimore County, Baltimore, MD 21250
e-mail: zliang@umbc.edu

Rupak K. Banerjee
Departments of Mechanical Engineering,
and Departments of Biomedical Engineering,
University of Cincinnati,
Cincinnati, OH 45221

Maher Salloum

Albert Bachmann

Department of Mechanical Engineering,
University of Maryland,
Baltimore County, Baltimore, MD 21250

Robert W. Flower
Departments of Ophthalmology,
New York University,
New York, NY;
Departments of Ophthalmology,
University of Maryland at Baltimore,
Baltimore, MD 21201

Laser photocoagulation of the feeder vessels of age-related macula degeneration-related choroidal neovascularization (CNV) membranes is a compelling treatment modality, one important reason being that the treatment site is removed from the fovea in cases of sub- or juxtafoveal CNV. To enhance the energy absorption in a target feeder vessel, an indocyanine green dye bolus is injected intravenously, and the 805 nm wavelength diode laser beam is applied when the dye bolus transits the feeder vessel; this tends to reduce concomitant damage to adjacent tissue. A 3D theoretical simulation, using the Pennes bioheat equation, was performed to study the temperature distribution in the choroidal feeder vessel and its vicinity during laser photocoagulation. The results indicate that temperature elevation in the target feeder vessel increases by 20% in dye-enhanced photocoagulation, compared to just photocoagulation alone. The dye bolus not only increases the laser energy absorption in the feeder vessel but also shifts the epicenter of maximum temperature away from the sensitive sensory retina and retinal pigment epithelial layers and toward the feeder vessel. Two dominant factors in temperature elevation of the feeder vessel are location of the feeder vessel and blood flow velocity through it. Feeder vessel temperature elevation becomes smaller as distance between it and the choriocapillaris layer increases. The cooling effect of blood flow through the feeder vessel can reduce the temperature elevation by up to 21% of the maximum that could be produced. Calculations were also performed to examine the effect of the size of the laser spot. To achieve the same temperature elevation in the feeder vessel when the laser spot diameter is doubled, the laser power level has to be increased by only 60%. In addition, our results have suggested that more studies are needed to measure the constants in the Arrhenius integral for assessing thermal damage in various tissues.
[DOI: 10.1115/1.2898832]

1 Introduction

Age-related macular degeneration (AMD) is the largest single cause of significant vision loss amongst patients aged 65 years and older in the United States. It is estimated that in the United States, more than 200,000 people develop it every year [1]. It is an unpredictable disease that attacks the sensory retina of the eye, affecting the macula and the fovea, those areas of the retina that afford acute central and color vision.

The anatomic structure of the posterior of the eye consists of multiple tissue layers, including the vitreous, retina and retinal vessels, retinal pigment epithelium (RPE), three layers of choroidal vessels: choriocapillaris, Sattlers's layer (the layer of midsized vessels in which most feeder vessels lie), and the large diameter vessels, and the sclera. Figure 1 compares the angioarchitecture of normal and AMD eyes. In the human eye, the central region of retina (~5.5 mm diameter) is called macula, and in the center of the macula is the fovea (~150–200 μm diameter). Since the fovea is avascular, all the nutrients to it are supplied by the underlying choriocapillaris, which is a thin (~10 μm) two-dimensional meshwork vascular structure, the choriocapillaries, consisting of all the capillaries of the choroidal vascular network. The choriocapillaris is supplied by numerous large diameter choroidal arteriolar vessels that connect to its posterior side and is drained by interspersed choroidal venous vessels. The major morphological change associated with 10% of the AMD cases is the formation of new vasculature arising from the anterior side of the choriocapillaries, and lying between it and the sensory retina (Fig. 1). The reason for this abnormal vascular growth, called choroidal neovascularization (CNV), is unknown; possibility it develops in response to some failure of the underlying choriocapillaries to provide adequate transport of nutrients and wastes to meet the metabolic demands of the overlying sensory retina. In any event, as the CNV develops its immature vessels leak fluid, producing edema that distorts the retinal tissue resulting in reduced visual acuity, and often these new vessels rupture, resulting in frank hemorrhage. In the extreme situation, formation of CNV can lead to retinal detachment and, again, loss of vision.

A number of methods have been developed for treatment of AMD-related CNV, including, for example, laser photocoagulation [2,3], surgical removal [4], macular translocation [5], photodynamic therapy, and various antiangiogenic drugs (the current
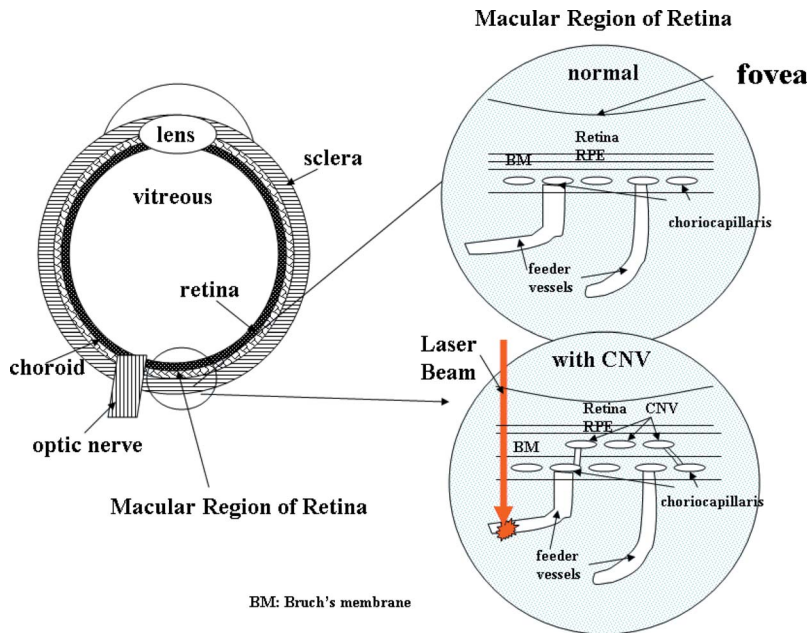

Fig. 1 Anatomy of the eye and vasculature of the choroid in the macular region

proliferation of these aims to counteract vascular endothelium growth factor, VEGF). Surgical extraction of subfoveal CNV has been demonstrated to preserve the remaining retinal function if the CNV is well defined, while the outcome is worse for ill-defined CNV [6]. Photodynamic therapy involves an intravenous injection of a photosensitive drug, which is activated by low dose of laser beam. Recent study has reconfirmed the benefits of photodynamic therapy in a retrospective review of this treatment. Only 24% of patients had moderate vision loss 12 months after the treatment [7]. Prompt laser photocoagulation is recommended based on the 5 year follow-up studies by the Macular Photocoagulation Study Group [8,9], which showed that laser photocoagulation of the well-defined extrafoveal, juxtafoveal, and subfoveal CNV secondary to AMD improved the visual outcome compared to the untreated group. However, direct and contiguous laser treatment of the entire subfoveal lesion almost invariably damages the foveal and macular region. Since the macula is responsible for central and color vision in human eyes, direct laser treatment is always associated with a substantial and immediate loss of central vision following the treatment. Loss of central vision may be due to direct damage to the foveal photoreceptors and RPE or from damage to the nerve fiber layer serving foveal function [10].

Indocyanine green (ICG) dye angiography is a clinical tool for diagnosis and management of CNV membranes secondary to AMD [1,11–13]. ICG dye is delivered to the eye via venous injection and reaches the large diameter choroidal vessels, the choriocapillaris, the CNV, and the retinal vessels at different times. The infrared absorption and emission spectra of ICG dye enable visualization and identification of the CNVs and their choroidal feeder vessels, having diameters of 50 μm or less. The term "feeder vessel" refers to any of those choroidal vessels in an ICG-dye angiogram image that appear to supply blood to the choriocapillaris in the vicinity of the CNV membrane origin.

Recently, laser photocoagulation techniques that attempt to spare the sensory retina adjacent to the treatment site have attracted a great deal of attention, particularly when the CNV is very near or underlies the fovea [11,14–18]. Since the blood supply to CNV membranes comes from the choriocapillaris, the hypothesis underlying this approach is that by selectively laser photocoagulating the choroidal vessels supplying blood to the choriocapillaries, it is possible to manipulate the blood pressure gradient within the choriocapillaris in such a way as to reduce or eliminate the hemodynamic force that drives blood through the CNV membrane. As shown in Fig. 1, a laser beam is aimed at a choroidal feeder vessel. Since the location of the laser interaction with the feeder vessel is away from the fovea and beneath the choriocapillaris, it is expected that the damage to the overlying RPE in the macular region is minimized. The feasibility of extrafoveal laser photocoagulation of the CNV feeder vessels has been demonstrated by several clinical studies in which the ICG-dye angiography was performed first to identify the choroidal feeder vessels perfusing each CNV membrane. The laser beam was then delivered to each target feeder vessel adjacent to the CNV to decrease the choriocapillaries blood pressure gradient in the vicinity of the CNV, and hence reduce blood flow in the CNV. Shiraga et al. [17] reported identifying feeding vessels in 37 of 170 consecutive patients (22%) and that photocoagulation of them resulted in resolution of the exudative manifestations. Improved or stabilized visual acuity in 70% of those 37 cases resulted from feeder vessel photocoagulation. Staurenghi et al. [18], also using the ICG-dye angiography-guided laser treatment of feeder vessels in AMD eyes, reported a success rate of 40% or higher. It was interesting to note that the success of obliteration of the CNV blood flow is strongly dependent on several factors such as feeder vessel width and length. Their success rate increased to 75% after selectively choosing patients with smaller feeder vessel diameters. A recent theoretical simulation by the authors [19] has confirmed the effectiveness of the feeder vessel photocoagulation approach. Using an anatomically realistic model based on the vascular cast of a human eye, blood flow simulations of partial and complete occlusions of a feeder vessel indicated that feeder vessel photocoagulation can lead to 75% reduction in the pressure gradient in the choriocapillaries and a concomitant 75% decrease in the CNV blood flow rate.

Although laser use in ophthalmology has a long history [20–25], most of the laser-based treatments depend on light/tissue interactions that occur in the superficial layers associated with the retina (neuroretina and RPE), not the deep choroidal layer containing the choroidal feeder vessels. In laser photocoagulation of feeder vessels, laser energy must penetrate the overlying retinal

layers, RPE, and choriocapillaris to reach and then be absorbed by the targeted feeder vessel. Energy absorption in the tissue or blood is largely dependent on the wavelength of the laser used; longer wavelengths penetrate more deeply onto tissue than short wavelengths. Therefore, it is logical to select a laser with a longer wavelength when deep tissue penetration is desired. Considering that the targeted vessels in these studies lie relatively deep, it is logical that the widely used 805 nm wavelength diode laser was selected as the source for maximizing energy absorption. An experimental study on pigmented rabbit eyes has shown that the photocoagulation of large choroidal arterioles can be accomplished with relatively little concomitant retinal tissue damage [16,26], when using near-infrared wavelengths, especially when used in conjunction with an injection biocompatible dye that enhances absorption of the laser energy.

Interestingly, ICG dye has an absorption peak near 800 nm wavelength that is very close to the emission peak of the near-IR wavelength diode laser (805 nm) used for the photocoagulation. The presence of ICG dye in the blood should enhance laser energy absorption, especially if the laser energy is applied precisely when a relatively concentrated dye bolus transits the targeted vessel. The special feature of ICG dye has been utilized in the past to enhance laser energy absorption in cancer treatment in combination with immunoadjuvant to stimulate an immune response [27] and in surgical endoscopy [28]. It is logical to expect enhancement in laser energy absorption in laser photocoagulation using ICG dye. Improved efficiency of CNV feeder vessel photocoagulation by this method has been demonstrated [16,26]. Although the preliminary experimental and clinical results have been promising, they have been achieved largely by trial and error and utilized somewhat unrefined approaches to determine what level of laser power to deliver. Providing the clinician with a way to calculate tissue temperature elevations achieved during photocoagulation would help address the uncertainty associated with determining optimal laser power levels to use, thereby making feeder vessel photocoagulation more efficacious, while improving patient safety and therapeutic outcome. Parametric numerical calculations could aid in the identification of the power delivery a priori for an improved and optimized treatment protocol.

In this study, a three-dimensional heat transfer model was developed to simulate the elevation in the temperature in the vicinity of a choroidal feeder vessel during dye-enhanced laser photocoagulation. This research focuses not only on the efficiency of ICG-dye enhancement in temperature elevation but also on the collateral damage to the RPE along the laser path. Parametric studies are performed to examine the effects of blood flow in a targeted vessel, laser power, laser spot size, and location of the feeder vessel on both the temperature rise and thermal damage to the surrounding tissues. Thermal damage to the feeder vessel assessed by the Arrhenius integration [29] is discussed.

2 Mathematical Formulation

2.1 Geometry. During feeder vessel laser photocoagulation, the laser beam penetrates different layers of eye tissue: vitreous, retina, RPE, choriocapillaris, Sattler's layer choroidal (wherein lie CNV feeder vessels), and sclera. Laser energy is absorbed in each layer and is also spread laterally in each layer. Considering the small size of the laser spot ($\sim$100 μm diameter) and the short duration of laser energy application ($\sim$1 s), one would expect tissue temperature elevation to be restricted within a very small lateral region in each layer. Therefore, in this study, the temperature distribution is simulated as a cylinder centered along the laser path. The diameter of the cylinder is selected to be 1 mm. As shown later in the results, the diameter is large enough so that the boundary condition on the cylinder surface will result in less than 0.1% change in the temperature elevation along the central line of the laser beam.

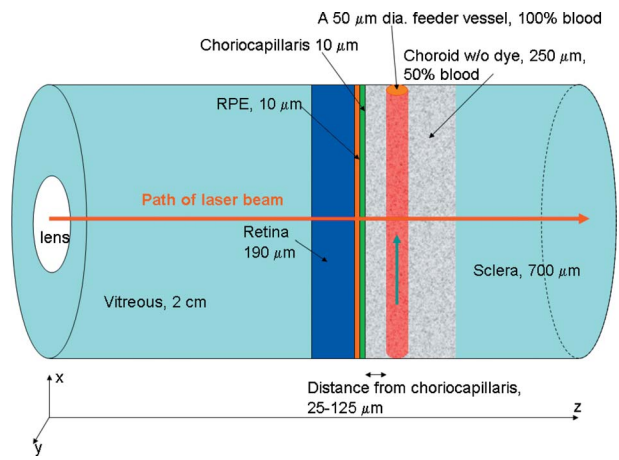Figure 2 shows the cross-sectional geometry of the eye along

Fig. 2 Three-dimensional geometrical representation of the eye in the heat transfer model and its coordinate system

the laser path. The laser beam passes along the central line of the temperature distribution cylinder; temperature elevation occurs in all the tissue layers along the laser path. Since the RPE has significantly different thermal absorption properties from that of the retina, it is modeled as an individual layer of 10 μm in thickness. As shown in Fig. 1, the choroidal feeder vessel (50 μm in diameter) usually rises obliquely to the $\sim$10 μm thick choriocapillaris layer. Thus, in this study the targeted choroidal feeder vessel is modeled as a tube of 50 μm in diameter embedded in the choroid and is placed perpendicularly to the laser path. The choroid is modeled as a single layer composed of 50% blood and 50% tissue.

2.2 Governing Equation. The three-dimensional Pennes bioheat equation in Cartesian coordinate system is used to model the temperature elevation in each layer and is given by

$$\rho c \frac{\partial T_t}{\partial t} = k_t \frac{\partial^2 T_t}{\partial x^2} + k_t \frac{\partial^2 T_t}{\partial y^2} + k_t \frac{\partial^2 T_t}{\partial z^2} + q_{laser} + \omega_b \rho_b c_b (T_a - T_t)$$

(1a)

where ρ is the density, c is the specific heat, T_t is the temperature of each layer, T_a is the arterial blood temperature of 37°C, and q_{laser} is the volumetric heat generation (W/m^3) modeling the laser energy absorption in each layer. Although a previous study [30] has suggested that a very minor role is played by the local blood perfusion rate ω_b, the effect of blood perfusion is modeled as a perfusion source term added to the traditional heat conduction equation. The governing equation for the temperature field in the feeder vessel includes the conduction and convection terms in the governing equation and is given by

$$\rho c \frac{\partial T_{feeder}}{\partial t} + u\rho c \frac{\partial T_{feeder}}{\partial x} = k_t \frac{\partial^2 T_{feeder}}{\partial x^2} + k_t \frac{\partial^2 T_{feeder}}{\partial y^2} + k_t \frac{\partial^2 T_{feeder}}{\partial z^2}$$
$$+ q_{laser,feeder}$$

(1b)

where u (m/s) is the average blood flow velocity of the feeder vessel.

2.3 Heat Source Distribution and Boundary and Initial Conditions. The heat generation term due to laser-tissue interaction depends on two parameters, namely, the fluence rate and the absorption coefficient. It is given by

$$q_{laser} = \mu I_{\lambda,r,z}$$

(2a)

where μ is the absorption coefficient, which depends on type of tissue and incident laser wavelength λ and $I_{\lambda,r,z}$ is the fluence rate (W/m^2). Here, r ($=\sqrt{x^2+y^2}$, in m) is the radial distance from the central line of the laser path. In this study, the laser travels along

the z axis. The fluence rate depends on many parameters, including laser intensity, spot diameter, and optical properties of tissues, such as scattering and absorption. If absorption *dominates* scattering ($\mu \gg \mu_s$) and the laser has uniform intensity along radial direction, the fluence rate is governed by the Beer–Lambert law as

$$I_{\lambda,z} = I_{\lambda,0}e^{-\mu z} \quad \text{for } \mu \gg \mu_s \tag{2b}$$

where $I_{\lambda,0}$ is the irradiation (W/m^2) obtained from incident laser power and z is the depth of the irradiated material (m). For materials whose *scattering is of the order of absorption*, the fluence rate predicted by the Beer–Lambert law may not be accurate [31,32]. Welch et al. [32] developed an alternative fluence rate based on combined scattering and absorption characteristics. They suggested the fluence rate for considerable scattering as

$$I_{\lambda,z} = I_{\lambda,0}e^{-(\mu+(1-g)\mu_s)z} \quad \text{for } \mu \sim \mu_s \tag{2c}$$

where g is the anisotropy factor, which is the cosine of average scattering angle. Thus, the variation of laser intensity along the radial direction depends on the profile of the beam. For top-hat profile, i.e., uniform intensity along radial direction, the heat source for a particular ocular tissue is

$$q_{\text{laser}} = \mu I_{\lambda,0}e^{-(\mu+(1-g)\mu_s)z} \tag{2d}$$

Since ocular tissues possess forward scattering characteristics (anisotropy factor g ranges from 0.85 to 0.97), the assumption holds good for ocular tissues [33]. Hammer et al. [33] employed double-integrating sphere technique and inverse Monte Carlo simulation to calculate the optical properties of ocular tissue. In order to predict the maximum temperature rise, the g value is considered to be 0.97 and thus, the effect of scattering is ignored for this study. Furthermore, since there were no previous experimental studies of the exact value of scattering coefficient, we used the values reported in Hammer et al. [33]. In the future, lower values of g such as 0.85 needs to be evaluated. Therefore, the volumetric heat generation in the tissue, q_{laser} (W/m^3), is simplified to

$$q_{\text{laser}} = I_{\lambda,0}\mu e^{-\mu z} \tag{3}$$

It may be noted that different layers of tissue may have different attenuation coefficients (μ), and $I_{\lambda,0}$ also varies for different layers due to the energy absorption in previous layers through which the laser beam has passed. A laser beam may process uniform or Gaussian profile. It is easily to obtain a uniform laser beam profile; however, a Gaussian beam is widely used. In this study, $I_{\lambda,0}$ has been assumed to be a Gaussian distribution in the radial direction (perpendicular to the light propagation, z) and is expressed as

$$I_{\lambda,0} = E_0 e^{-r^2/W_L^2} \tag{4}$$

where r ($r = \sqrt{x^2+y^2}$) is the radial distance from the central line of the laser path, E_0 (W/m^2) is the maximum irradiance and is related to the total laser power, and W_L is the $1/e^2$ radius of the laser beam. Based on the above derivation, the volumetric heat generation rate by laser in each layer is expressed by

$$q_{\text{laser,vitreous}} = E_0\mu_{\text{vitreous}}e^{-r^2/W_L^2}e^{-\mu_{\text{vitreous}}z} \tag{5a}$$

$$q_{\text{laser,retina}} = E_0\mu_{\text{retina}}e^{-r^2/W_L^2}e^{-\mu_{\text{vitreous}}h_{\text{viteour}}}e^{-\mu_{\text{retina}}(z-h_{\text{vitreous}})} \tag{5b}$$

$$q_{\text{laser,RPE}} = E_0\mu_{\text{RPE}}e^{-r^2/W_L^2}e^{-\mu_{\text{vitreous}}h_{\text{viteour}}}e^{-\mu_{\text{retina}}h_{\text{retina}}}$$
$$\times e^{-\mu_{\text{RPE}}(z-h_{\text{vitreous}}-h_{\text{retina}})} \tag{5c}$$

$$q_{\text{laser,CC}} = E_0\mu_{\text{CC}}e^{-r^2/W_L^2}e^{-\mu_{\text{vitreous}}h_{\text{viteour}}}e^{-\mu_{\text{retina}}h_{\text{retina}}}$$
$$\times e^{-\mu_{\text{RPE}}h_{\text{RPE}}}e^{-\mu_{\text{CC}}(z-h_{\text{vitreous}}-h_{\text{retina}}-h_{\text{RPE}})} \tag{5d}$$

$$q_{\text{laser,feeder}} = E_0\mu_{\text{feeder}}e^{-r^2/W_L^2}e^{-\mu_{\text{vitreous}}h_{\text{viteour}}}e^{-\mu_{\text{retina}}h_{\text{retina}}}e^{-\mu_{\text{RPE}}h_{\text{RPE}}}$$
$$\times e^{-\mu_{\text{CC}}h_{\text{CC}}}e^{-\mu_{\text{choroid}}h_{\text{gap}}}e^{-\mu_{\text{feeder}}(z-h_{\text{vitreous}}-h_{\text{retina}}-h_{\text{RPE}}-h_{\text{CC}}-h_{\text{gap}})} \tag{5e}$$

$$q_{\text{laser,choroid}} = E_0\mu_{\text{feeder}}e^{-r^2/W_L^2}e^{-\mu_{\text{vitreous}}h_{\text{viteour}}}e^{-\mu_{\text{retina}}h_{\text{retina}}}$$
$$\times e^{-\mu_{\text{RPE}}h_{\text{RPE}}}e^{-\mu_{\text{CC}}h_{\text{CC}}}e^{-\mu_{\text{choroid}}(z-h_{\text{vitreous}}-h_{\text{retina}}-h_{\text{RPE}}-h_{\text{CC}})} \tag{5f}$$

$$q_{\text{laser,sclera}} = E_0\mu_{\text{sclera}}e^{-r^2/W_L^2}e^{-\mu_{\text{vitreous}}h_{\text{viteour}}}e^{-\mu_{\text{retina}}h_{\text{retina}}}e^{-\mu_{\text{RPE}}h_{\text{RPE}}}$$
$$\times e^{-\mu_{\text{CC}}h_{\text{CC}}}e^{-\mu_{\text{choroid}}h_{\text{choroid}}}$$
$$\times e^{-\mu_{\text{sclera}}(z-h_{\text{vitreous}}-h_{\text{retina}}-h_{\text{RPE}}-h_{\text{CC}}-h_{\text{choroid}})} \tag{5g}$$

In Eq. (5a), the laser beam impinges on the vitreous surface at $z=0$. A simple derivation has shown the relationship between the maximum irradiance E_0 at $z=0$ and the laser power level Q to be

$$Q = \pi W_L^2 E_0 \tag{6}$$

At the interface between any two tissue layers, temperature and heat flux continuities are maintained. The temperatures at all boundary surfaces are 37°C. The temperature field is initially uniform at 37°C. The ICG-dye-enhanced laser energy absorption is modeled as an increase in the attenuation coefficient in the feeder vessel.

All the finite element calculations including the finite element mesh generation are performed on FEMLAB 3.1, operated on a Pentium IV processor of 2.79 GHz speed, and using 2 Gbytes of memory under a WINDOWS XP SP2 Professional Operating System. The numerical model was obtained by applying the Galerkian formulation to Eqs. (1a) and (1b). The total number of tetrahedral elements of the finite element mesh is around 850,000. The time dependent problem was solved using an adaptive time stepping scheme wherein the convergence criterion was kept at 10^{-6}. Mesh independency was checked by increasing the number of elements in the feeder vessel by 10% over the current mesh. The finer mesh showed less than 1% difference in the temperature field. The mesh size could not be further deceased, since the finer mesh resolution reached the maximum capacity supported by the computer's internal memory of 2 Gbytes.

2.4 Thermal Damage. It is well known that heat-induced tissue damage depends on heating history, which includes both the tissue temperature elevation and heating duration. Moritz and Henriques [34] originally assumed that the kinetics of the thermal destruction process in living tissues is similar to the first order chemical reaction process. This assumption later became the standard for thermal injury evaluation. Based on this assumption, the thermal damage to tissue is evaluated by means of the Arrhenius integral Ω:

$$\Omega(x,y,z,t) = A\int_0^t e^{-E_a/R_u T_t(x,y,z,t)}dt \tag{7}$$

where A is the frequency or preexponential factor (1/s), E_a is the activation energy barrier (J/mole), R_u is the universal gas constant (8.32 J/mole K), and $T_t(x,y,z,t)$ is the absolute tissue temperature at location (x,y,z) [35]. The value of Ω is zero before application of the heat-producing laser energy, and it increases during heating. 63% and 98% denaturations of protein occur when $\Omega = 1$ and 4, respectively. Numerical simulations make it possible to assess the potential thermal damage after the laser treatment. The temperatures determined in the study $T_t(x,y,z,t)$ can then be substituted into the integral in Eq. (7) to assess the degree of thermal damage.

Table 1 Geometrical parameters and optical properties of eye tissues

	Thickness h (m)	Attenuation coefficient μ (1/m)	Blood perfusion rate ω ((1/s) or (ml/min.100 g))
Vitreous	0.02	2.56	0
Retina	0.00019	725	0.005 (30)
RPE	0.00001	14,000	0.005 (30)
Choriocapillaris	0.00001	2,040	0.167 (1000)
Choroid feeder vessel	0.00005	4,610 (without dye), 9,000 (with dye)	0
Choroid	0.00025	3,500	0.005 (30)
Sclera	0.0007	506	0.00046 (2.7)

3 Results

3.1 Parameters and Thermal Properties. The laser spot has a $1/e^2$ radius of 50 μm (W_L). Table 1 lists the geometrical parameters, radiation properties, and local blood perfusion rate of each layer used in the model. It may be noted that the total thickness of the choroid is 250 μm. The choroidal feeder vessel can be located close to or far away from the posterior surface of the choriocapillaries, so that the distance between the choriocapillaris and the anterior surface of the choroidal feeder vessel, h_{gap}, was selected to be 25 μm, 50 μm, 75 μm, 100 μm, or 125 μm.

The attenuation coefficient in the vitreous layer ($\mu_{vitreous}$) was derived based on previous result that only 5% of laser energy at 810 nm wavelength is absorbed in this layer [36]. The RPE has the highest attenuation coefficient of around 14,000 m^{-1}. ICG-enhanced laser absorption in the feeder vessel was modeled as an increase in the attenuation coefficient from 4610 m^{-1} to 9000 m^{-1}, as shown in Flower [26]. The attenuation coefficient in the retinal layer is similar to that in the layer of sclera [37].

Local blood perfusion rate in each layer is listed in Table 1. The choriocapillaris has the highest rate of volume blood flow per tissue weight of any tissue structure in the human body. The value of 0.167 s^{-1} in choriocapillaris is equivalent to 1000 ml/min.100 g tissue. On the other hand, the local blood perfusion rate in the sclera is around 3 ml/min. 100 g tissue, which is similar to that in resting muscle. The high demand in nutrients in the retina, RPE, and choroid requires a high blood perfusion rate. In this study, the values selected for these three tissue layers were 0.005 s^{-1}, or 30 ml/min. 100 g tissue, as used in a previous study [38]. Table 2 gives the values of a base line combination of parameters used in the computations. The laser beam was 100 μm diameter with a power level of 0.05 W. The total heating duration was 1 s.

3.2 Baseline Temperature Field With Enhanced Energy Absorption by ICG Dye. Figures 3(a) and 3(b) show the temperature contours in the vicinity of the choroidal feeder vessel without and with ICG-dye-enhanced energy absorption, respectively. Temperature contours are similar in both images except that the temperature elevations in the feeder vessel are smaller when no ICG dye is added to the blood stream. The temperature field in the vicinity of the feeder vessel is enlarged and shown in Fig. 3(c). Maximum temperatures in most of the layers occur at the center of the laser spot. However, in the axial direction of the feeder vessel, the maximum temperature shifts toward downstream in the vessel due to the heat convection in the x direction. Temperature

Table 2 Parameters of the base line model

$Q=0.05$ W	$W_L=50$ μm	$I_0=637$ W/cm^2	$u=8$ mm/s
$\Delta t=1$ s	$\mu_{feeder}=9000$ m^{-1}	$h_{gap}=75$ μm	

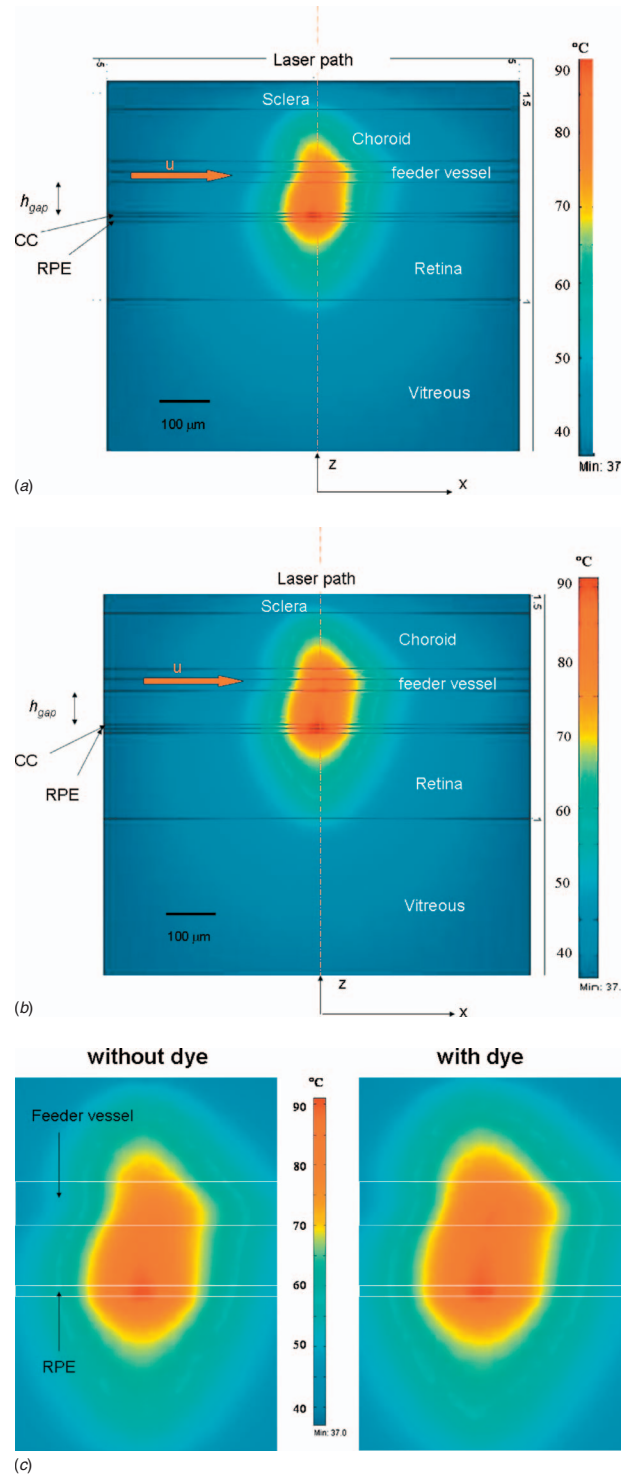**Fig. 3 Contour plot of the temperature distribution in the vicinity of the feeder vessel at the end of the heating duration ($t=1$ s): (a) without dye; (b) with dye; (c) enlarged temperature contours in the vicinity of the feeder vessel**

distribution is not axisymmetric about the central line of the laser path due to the blood flow in the feeder vessel. The original selection of the size of the simulated domain (1 mm diameter cylinder) is large enough so that the boundary condition at the cylinder surface did not interfere with the temperature elevation in the center region.

The transient behavior of the temperature elevations in three tissue locations are examined in Fig. 4. At the beginning of the
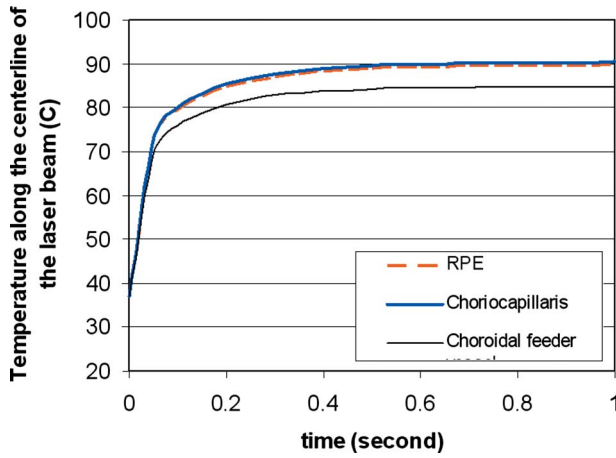
Fig. 4 Temperature rises in RPE, choriocapillaries, and choroidal feeder vessel during the heating

Fig. 6 Lateral temperature distributions in the axial direction of the feeder vessel. Note the change in the FWHM under different blood flow velocities.

heating ($t < 0.05$ s), a linear temperature elevation is observed, which indicates that initial heat conduction can be neglected. However, for the majority of the heating durations ($1.0 \geq t \geq 0.05$ s), temperature rises slowly. This result suggests that heat conduction and convection in the tissue play important roles as heating continues.

Heat is conducted along the laser path as well as in the x and y planes. Figures 5 and 6 examine the effect of blood flow in the feeder vessel. The lateral temperature profiles in the y direction are plotted in Fig. 5. It may be noted that the feeder vessel is placed parallel to the x axis; a symmetric temperature distribution is observed. As expected, the effect of the blood flow velocity is to lower the temperature elevation. The full width of half maximum (FWHM) in the y direction at the choroidal feeder vessel is approximately 190 μm when the laser spot is 100 μm in diameter. The FWHM varies between 176 μm and 200 μm over the range of the blood flow velocity. If the choroidal feeder vessel is less than 25 μm in radius (50 μm diameter shown by the circle in Fig. 5) and the laser is aimed at the center of the feeder vessel, temperature elevation in the feeder vessel is almost uniform. As shown in Fig. 6, the temperature distribution along the feeder vessel (x direction) is asymmetric and the maximum temperature

shifts from the center of the laser spot to the downstream due to the heat convection in the feeder vessel. The enhancement in heat transfer in the x direction due to the blood flow results in a reduction of focused temperature rise at the laser spot than that when $u = 0$. Consequently, a larger FWHM is observed in the x direction than that in the y direction (240 μm versus 200 μm when $u = 15$ mm/s).

The convective effect is further examined in Fig. 7, where the temperature elevation at the end of the heating period at the center of the feeder vessel is plotted to illustrate the effect of blood flow velocity on the temperatures. Blood flow in vessels usually acts as a heat sink resulting in thermal cooling during laser treatment. The cooling effect due to the heat convection by the blood flow is relatively small ($7 \,^{\circ}$C) when heat conduction is not dominant, while it increases to more than $11 \,^{\circ}$C at the end of the heating period ($t = 1$ s). The temperature elevation without the blood flow is approximately $52 \,^{\circ}$C, and it drops 21% to $41 \,^{\circ}$C when $u = 15$ mm/s.

3.3 Temperature Elevation in Different Tissue Layers and the Effect of Dye-Enhanced Energy Absorption. Detailed temperature profiles along the central line of the laser path ($r = 0$) are illustrated in Figs. 8(a) and 8(b) for the normal and ICG-dye-enhanced conditions, respectively. Since temperature elevations in the vitreous, retina, and sclera are relatively minor (less than 15% of the maximum temperature rise), only the temperature profile in the vicinity of the choroidal feeder vessel is discussed. Temperature elevations of $52 \,^{\circ}$C and $42 \,^{\circ}$C are observed in the RPE and the feeder vessel, respectively, for the normal condition (Fig.
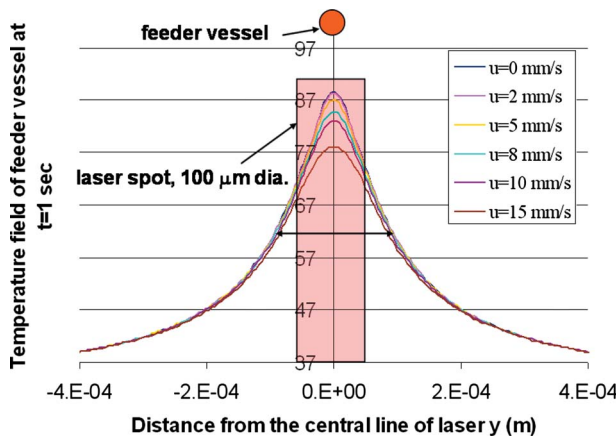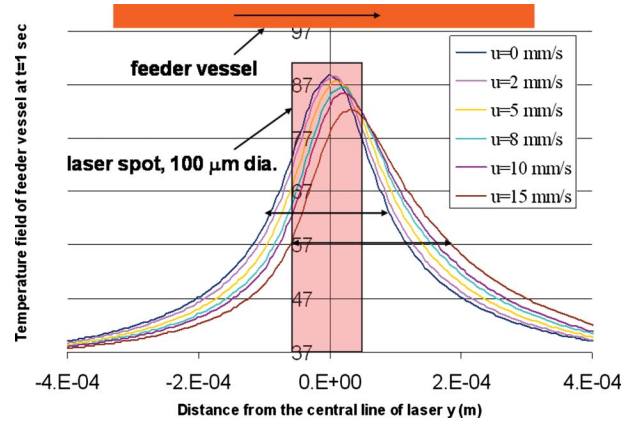

Fig. 5 Lateral temperature distributions from the center of the choroidal feeder vessel in the y direction as a function of the blood flow velocity in the vessel. The red circle represents the feeder vessel and the pink area refers to the region covered by the laser spot. The FWHM is denoted by the double arrows.
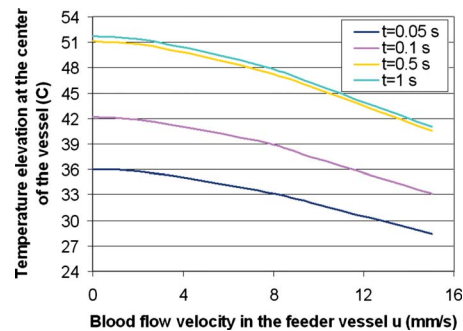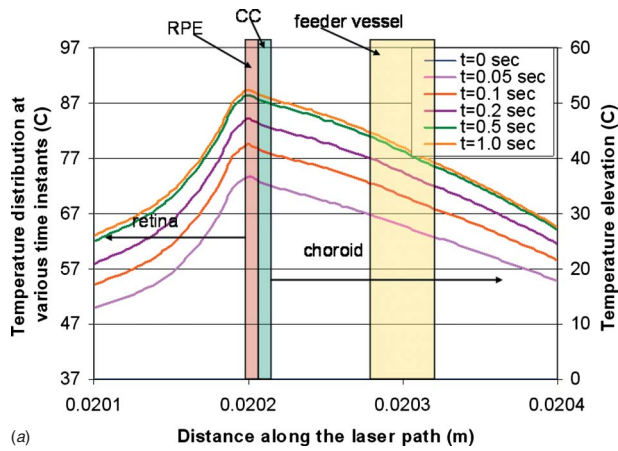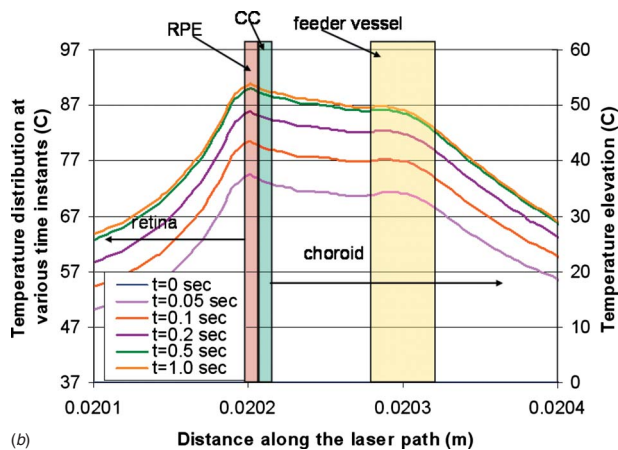

Fig. 7 Temperature elevations at the center of the choroidal feeder vessel as a function of the blood flow velocity when $t = 1$ s

(a)

(b)

Fig. 8 Temperature profiles and temperature rises along the laser path at different time instants: (*a*) without dye; (*b*) with dye

8(*a*)). The dye-enhanced energy absorption in the feeder vessel results in a temperature elevation of 49°C, a 20% increase from the normal condition, as shown in Fig. 8(*b*). Temperature elevation at the RPE also increases slightly (53°C) from the normal condition. It is evident from these two figures that the ICG-dye-enhanced energy absorption results in a higher temperature elevation in the feeder vessel. The ratio of temperature rise in the RPE to that in the feeder vessel, $\beta = \Delta T_{\mathrm{RPE}} / \Delta T_{\mathrm{feeder}}$ is introduced to evaluate collateral damage occurring in the RPE. Based on the data given in Figs. 8(*a*) and 8(*b*), one can calculate that β decreases from 1.24 (=52°C/42°C) in the normal condition to 1.08 (=53°C/49°C) in the dye-enhanced condition.

3.4 Effect of Feeder Vessel Distance From the Choriocapillaris. In order to preserve the RPE overlying sub- or juxtafoveal CNV, in clinical and animal studies of feeder vessel laser photocoagulation, the feeder vessel laser target site is chosen to be away from the fovea [26] (see Fig. 1). As a first approximation, since feeder vessels rise obliquely toward the choriocapillaris, the distance between the targeted site on a feeder vessel and the choriocapillaris may become greater as the target site is moved away from the fovea.

The effect of the distance, h_{gap}, on the temperature elevation of the feeder vessel is shown in Fig. 9 when the thickness varies between 25 μm and 125 μm. The major role played by h_{gap} is to make the energy absorption less concentrated in the area surrounding the RPE. Therefore, the maximum temperature elevation in the feeder vessel decreases as h_{gap} increases. One observes a
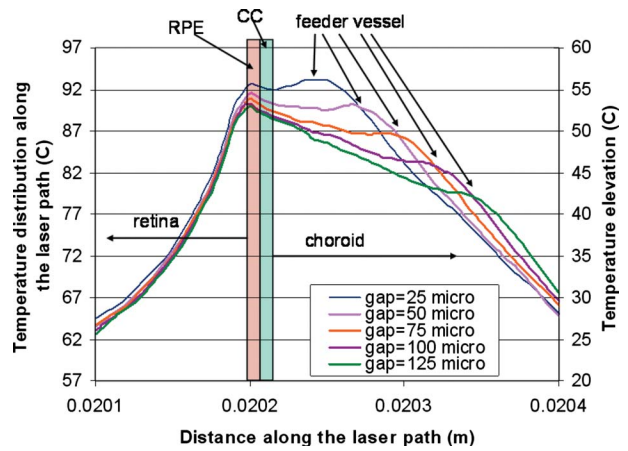

Fig. 9 Effect of the location of the feeder vessel on the temperature profile along the laser path

significant increase in $\Delta T_{\mathrm{feeder}}$ and a relatively minor increase in the temperature elevation at the RPE and choriocapillaris as the site on the feeder vessel moves closer to the choriocapillaris in Fig. 9. When the feeder vessel site is very close to the choriocapillaris, the temperature elevation in the feeder vessel is higher than that in the sensitive RPE region. The value of β keeps decreasing as h_{gap} decreases in the ICG-dye-enhanced case. β drops from 1.23 ($h_{\mathrm{gap}} = 125$ μm) to 1.15 ($h_{\mathrm{gap}} = 100$ μm), to 1.06 ($h_{\mathrm{tissue}} = 75$ μm), to 1.00 ($h_{\mathrm{tissue}} = 50$ μm), and finally to 0.97 when the distance is 25 μm. Selecting a focused site along the vessel in the attempt to be as far as possible from the choriocapillaris would result a small temperature rise, and the collateral damage to the RPE would be relatively large, since more laser power would be needed to elevate the temperature of the feeder vessel.

3.5 Effect of Laser Spot Size and Temperature Level. Figure 10 examines the effect of the size of the laser spot on temperature elevation of the feeder vessel. Doubling the spot size reduces the maximum temperature elevation by only 40% when the laser power is kept the same. In order to achieve the same level of maximum temperature elevation at the center of the feeder vessel, the power level must be increased from 0.05 W to 0.08 W to compensate for the less focused heating area. As also shown in Fig. 10, the temperature elevation is almost proportional to the laser power level if all the other parameters are unchanged.
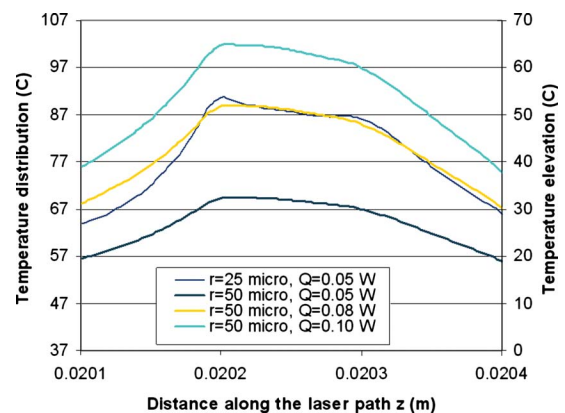

Fig. 10 Effects of the diameter of the laser spot and the laser power on the temperature profiles along the laser path

Table 3 Thermal damage Ω in the feeder vessel and RPE

Time t (s)	0.1	0.2	0.4	0.5	1.0
Feeder vessel	0.01	0.5	2.6	3.9	12.1
RPE	0.03	1.5	8.3	13.3	43.6

Arrhenius Integral Thermal Damage of the Feeder Vessel. To assess the tissue damage to the feeder vessel, both constants A and E_a in Eq. (7) are needed. They have been well reported for temperatures much less than $100\,^\circ$C. In this study, the Arrhenius integral was estimated based on the data given by Birngruber et al. [39], where $A=10^{66}$ (1/s) and $E_a=2.93\times10^5$ J/mole K. Applying the simulated temperature history using the parameters of the base line model and assuming that the Arrhenius constants are unchanged during heating, the values of Ω for the feeder vessel and RPE were calculated for different points in time. Table 3 gives the Arrhenius integral as a function of the heating duration. Under the current laser power level, the heating duration has to be longer than 0.5 s for $\Omega>4$. $\Omega=4$ corresponds to a 98% denaturation of tissue.

Under the assumption that the Arrhenius constants are the same to both the RPE and feeder vessel, the calculated Ω at the RPE was almost three times of that at the feeder vessel. The huge difference of Ω between the two values is the direct result of the exponential relationship between the temperature and the Arrhenius integral, even if the temperature elevation in the RPE is only 8% higher than that in the feeder vessel. In the temperature range when both A and E_a are relatively unchanged, the Arrhenius integral suggested that when the temperature elevation is increased by $1\,^\circ$C (or Kelvin) the heating duration can be halved to achieve the same degree of thermal damage [40]. However, this result is contrary to the consistent clinical observation that, by using ICG-dye-enhanced photocoagulation, CNV feeder vessels are closed without visible damage to the overlying RPE. This disparity suggests that the Arrhenius constants used to estimate thermal damage at the RPE may be different from that of the feeder vessel. Moreover, the assumption that the Arrhenius constants do not change during heating may be incorrect. Further studies of quantification of the Arrhenius constants are warranted to improve the accuracy of assessing thermal damage in tissue.

4 Discussion

The current simulation provides insights on the laser photocoagulation treatment protocols that have been used in clinical studies. The FWHM is approximately 200 μm in radius when the laser spot size is 100 μm in diameter. If the laser beam can be aimed at the center of the feeder vessel, the temperature elevation in the feeder vessel will be almost uniform. As practiced in the great majority of cases, during CNV feeder vessel laser photocoagulation, the ophthalmologist cannot actually "see" the feeder vessel when the laser energy is applied, as he/she applies laser energy to the eye using a slit-lamp delivery system that affords only a reflected-white-light visualization of the fundus; he must rely on using the visible retinal vessels as a road map to decide where to apply laser energy, based on a previously recorded ICG angiogram image that shows the major retinal vessels in relationship to the underlying choroidal vessels, including the target CNV feeder vessel. Although this method of feeder vessel treatment has proven to be effective, there is always a question as to the accuracy with which photocoagulation laser energy has been applied. As shown in the theoretical simulation, if the laser is aimed 100 μm from the center of the feeder vessel, temperature elevation will be significantly reduced and the effectiveness of the thermal therapy will be compromised. As a consequence, either the laser power level or the heating duration would have to be increased to a much higher level to successfully photocoagulate the targeted vessel, and that inevitably would cause unnecessary col-

lateral damage to the RPE and sensory retina. This study indicates the consequences of imperfect laser energy application in terms of achieving consistent clinical results.

Unlike pulsed laser treatment [41], in which heat conduction and convection do not play a significant role in determining the temperature elevation, blood flow in the feeder vessel is one of the dominant factors that can affect the treatment efficiency of the laser photocoagulation. Heat convection in the axial direction of the feeder vessel causes the thermal energy to be less concentrated within the laser spot, and therefore, a smaller temperature elevation would occur at the targeted feeder vessel as a result of blood mass movement during laser energy application. Depending on the blood flow velocity, the effect of the blood flow can lower the temperature rise by 21%. However, during the current treatment protocols using laser therapy, the blood flow velocity is usually unknown to the ophthalmologist. A recent paper by the authors [42] has provided a quantitative estimate of the blood flow velocity based on the ICD dye angiograms performed routinely for AMD patients. If this approach of measuring the blood flow velocity in the targeted feeder vessel can be combined with the laser therapy, the current CNV feeder vessel laser treatment for AMD patients can be greatly improved to deliver a precise thermal dose while minimizing collateral tissue damage.

This research confirms that ICG-dye-enhanced laser photocoagulation will result in a higher temperature elevation in a choroidal feeder vessel. If the feeder vessel is located relatively far away from the choriocapillaris, the enhancement in the laser energy absorption would result in a small increase in the temperature elevation at the RPE. One way to further boost the energy absorption is to increase the concentration of the dye bolus that is injected, assuming that it can be done safely in the patient. In theory, a further increase in the dye concentration has the potential to shift the maximum temperature from the RPE and sensory retina toward the feeder vessel.

If ICG-dye-enhanced photocoagulation is practiced using the slit-lamp delivery system, where the feeder vessel cannot be directly visualized, one technical issue facing the ophthalmologist is the precise timing of the arrival of the dye bolus at the targeted feeder vessel to exploit the dye-enhanced energy absorption. In the clinical studies, the ophthalmologist estimates the time for the dye bolus traveling to the targeted choroidal feeder vessel based on the angiogram obtained before the laser therapy. After the ICG-dye angiogram, the same amount of dye is injected intravenously again to the patient and laser is delivered after that specific time interval. Since the dye bolus travels relatively fast in the choroidal feeder vessel ($\sim$2 mm/s) [42], missing the dye bolus during its transit through the targeted vessel would result in a smaller temperature elevation, as shown by the simulation for the normal condition.

One motivation of CNV feeder vessel laser photocoagulation is to avoid thermal damage to the RPE in the macular region by shifting the laser path away from the macula. The size of macula is approximately 100 μm in radius. The center of a laser spot of 50 μm in radius should be placed at least 150 μm (50+100) away from the fovea. If the rising angle of the feeder vessel is approximately 45 deg, the tissue gap between the focus point at the feeder vessel and the RPE should be at least 150 μm. However, if the feeder vessel rises almost parallel to the choriocapillaris, the tissue gap would be smaller. As suggested by Fig. 9, the collateral damage to the RPE will be smaller if the laser spot is relatively closer to the choriocapillaris. Nevertheless, under the current base line parameters, thermal damage to the densely pigmented RPE along the laser path is inevitable for the selected laser parameters due to the high laser energy absorption by the pigment in this layer; the results also indicate that when using dye-enhanced photocoagulation, temperature elevation at the feeder vessel increases by 20%, without concomitant significant elevation of RPE temperature. It is conceivable that further boost in feeder vessel temperature rise produced by dye-enhanced photocoagulation may be feasible by

increasing the concentration of the transiting dye bolus, by modifying the dye injection regimen, or by modifying the absorption characteristics of the dye bolus by some means. Since both dye-enhanced energy absorption and the location of the feeder vessel photocoagulation site can affect the degree of collateral RPE damage, future clinical protocols could be improved not only by increasing the dye concentration but also by selecting photocoagulation sites closer to the choriocapillaris so that the maximum temperature would shift farther from the RPE to the feeder vessel.

This theoretical analysis is limited by the simplification of the choroidal feeder vessel as a straight tube placing perpendicular to the laser path. Since this is a three-dimensional heat transfer model, a more accurate representation of the vasculature would require far more intensive computational resources. As shown in the simulation of the radial temperature distribution, significant temperature elevation is limited to a cylinder of less than 200 μm (FWHM) in radius. Nevertheless, we believe that the model simulation may still be faithful to the clinical situation due the small focus area of the laser spot and the short time duration of the heating. This can certainly be tested in the future when a more powerful computer simulation is available.

In summary, in this study a theoretical simulation is performed to predict the temperature field in the vicinity of the choroidal feeder vessel during CNV feeder vessel laser photocoagulation. ICG-dye-enhanced laser photocoagulation increases the temperature rise at the targeted vessel region. Less collateral damage is induced to the RPE with dye-enhanced energy absorption in the feeder vessel and when the targeted feeder vessel site is closer to the RPE. We believe that this study helps in providing valuable information to ophthalmologists in designing and optimizing the treatment protocol to patients with AMD-relation CNV, especially under conditions where real-time image technique of the targeted feeder vessel and the transit of the ICG-dye bolus is available during the laser energy application.

Acknowledgment

Nomenclature

A = frequency or preexponential factor (1/s)
c = specific heat capacity (J/kgK)
E_a = activation energy (J/mol)
E_0 = maximal irradiance at $r=0$ (W/m^2)
h = thickness of each structure (m)
h_{gap} = distance between the bottom of choriocapillaris and the top surface of the feeder vessel
I = irradiance of the laser (W/m^2)
k = thermal conductivity (W/m K)
r = Radial distance from the central line of the laser path (m)
q_{laser} = volumetric heat generation rate (W/m^3)
Q = laser power (W)
T = temperature (°C or K)
W_L = $1/e^2$ radius of the laser beam
x, y, z = Cartesian coordinate system

Greek Letters

ρ = density of tissue (kg/m^3)
μ = attenuation coefficient due to absorption and scattering (1/m)
Ω = Arrhenius integral
β = ratio of temperature rise in the RPE to that in the feeder vessel

Subscript

a = artery
b = blood
cc = choriocapillaris
t = tissue

References

[1] Lewis, H., 1988, "Subfoveal Choroidal Neovascularization: Is There a Role for Submacular Surgery," Am. J. Ophthalmol., **126**, pp. 127–129.
[2] Asrani, S., Zou, S., D'Anna, S., Phelan, A., Goldberg, M., and Zeimer, R., 1996, "Selective Visualization of Choroidal Neovascular Membranes," Invest. Ophthalmol. Visual Sci., **37**, pp. 1642–1650.
[3] Schneider, S., Greven, C. M., and Green, W. R., 1998, "Photocoagulation of Well-Defined Choroidal Neovascularization in Age-Related Macular Degeneration," Retina, **18**, pp. 242–250.
[4] Submacular Surgery Trials Pilot Study Investigators, 2000, "Submacular Surgery Trials Randomized Pilot Trial of Laser Photocoagulation Versus Surgery for Recurrent Choroidal Neovascularization Secondary to Age-Related Macular Degeneration: I. Ophthalmic Outcomes," Am. J. Ophthalmol., **130**, pp. 387–407.
[5] Lewis, H., Kaiser, P. K., Lewis, S., and Estafanous, M., 1999, "Macular Translocation for Subfoveal Choroidal Neovascularization in Age-Related Macular Degeneration: A Prospective Study," Am. J. Ophthalmol., **128**, pp. 135–146.
[6] Scheider, A., Gundisch, O., and Kampik, A., 1999, "Surgical Extraction of Subfoveal Choroidal New Vessels and Submacular Haemorrhage in Age-Related Macular Degeneration: Results of a Prospective Study," Graefe's Arch. Clin. Exp. Ophthalmol., **237**(1), pp. 10–15.
[7] Sharp, D. M., Lai, S., and Markey, C. M., 2007, "Photodynamic Therapy With Verteporfin for Choroidal Neovascularization Due to Age-Related Macular Degeneration and Other Causes: A New Zealand Outcomes Study," Clin. Exp. Ophthalmol., **35**(1), pp. 24–31.
[8] Macular Photocoagulation Study Group, 1993, "Five-Year Follow-up of Fellow Eyes of Patients With Age-Related Macular Degeneration and Unilateral Extrafoveal Choroidal Neovascularization," Arch. Ophthalmol. (Chicago), **111**, pp. 1189–1199.
[9] Macular Photocoagulation Study Group, 1993, "Laser Photocoagulation of Subfoveal Neovascular Lesions of Age-Related Macular Degeneration," Arch. Ophthalmol. (Chicago), **111**, pp. 1200–1209.
[10] Ham, W. T., Mueller, H. A., Wolbarsht, M. L., and Sliney, D. H., 1988, "Evaluation of Retinal Exposures From Repetitively Pulsed and Scanning Lasers," Health Phys., **54**(3), pp. 337–344.
[11] Reichel, E., Puliafito, C. A., Duker, J. S., and Guyer, D. R., 1994, "Indocyanine Green Dye-Enhanced Diode Laser Photocoagulation of Poorly Defined Subfoveal Choroidal Neovascularization," Ophthalmic Surg., **25**, pp. 195–201.
[12] Kramer, M., Mimouni, K., Priel, E., Yassur, Y., and Weinberger, D., 2000, "Comparison of Fluorescein Angiography and Indocyanine Green Angiography for Imaging of Choroidal Neovascularization in Hemorrhagic Age-Related Macular Degeneration," Am. J. Ophthalmol., **129**, pp. 495–500.
[13] Weinberger, A. W. A., Knabben, H., Solbach, U., and Wolf, S., 1999, "Indocyanine Green Guided Laser Photocoagulation in Patients With Occult Choroidal Neovascularization," Br. J. Ophthamol., **83**, pp. 168–172.
[14] Falcone, P., Chaudhry, N. A., and Grannum, E., 1998, "Perifoveal Laser Treatment for Subfoveal Choroidal Neovascularization in Age-Related Macular Degeneration," Ophthalmic Surg. Lasers, **29**, pp. 933–934.
[15] Flower, R. W., 1999, "Expanded Hypothesis on the Mechanism of Photodynamic Therapy Action on Choroidal Neovascularization," Retina, **19**(5), pp. 365–369.
[16] Flower, R. W., 2000, "Experimental Studies of Indocyanine Green Dye-Enhanced Photocoagulation of Choroidal Neovascularization Feeder Vessels," Am. J. Ophthalmol., **129**, pp. 501–512.
[17] Shiraga, F., Ojima, Y., Matsuo, T., Takasu, I., and Matsuo, N., 1998, "Feeder Vessel Photocoagulation of Subfoveal Choroidal Neovascularization Secondary to Age-Related Macular Degeneration," Ophthalmology, **105**, pp. 662–669.
[18] Staurenghi, G., Orzalesi, N., La Capria, A., and Aschero, M., 1998, "Laser Treatment of Feeder Vessels in Subfoveal Choroidal Neovascular Membranes," Ophthalmology **105**, pp. 2297–2305.
[19] Flower, R. F., Von Kerczek, C., Zhu, L., Earnest, A., Eggleton, C., and Topoleski, L. D. T., 2001, "A Theoretical Investigation of the Role of Choriocapillaris Blood Flow in Treatment of Sub-Foveal Choroidal Neovascularization Associated with Age-Related Macular Degeneration," Am. J. Ophthalmol., **132**, pp. 85–93.
[20] Berger, J. W., 1997, "Thermal Modeling of Micropulsed Diode Laser Retinal Photocoagulation," Lasers Surg. Med., **20**, pp. 409–415.
[21] Mainster, M. A., White, T. J., Tips, J. H., and Wilson, P. W., 1970 "Retina-Temperature Increases Produced by Intense Light Sources," J. Opt. Soc. Am., **60**(2), pp. 264–270.
[22] Mainster, M. A., White, T. J., and Allen, R. G., 1970, "Spectral Dependence of Retina Damage Produced by Intense Light Sources," J. Opt. Soc. Am., **60**(6), pp. 848–855.
[23] White, T. J., Mainster, M. A., Tips, J. H., and Wilson, P. W., 1970, "Chorioretinal Thermal Behavior," J. Inf. Technol. Teach. Educ., **32**, pp. 315–322.
[24] Van Gemert, M. J. C., and Welch, A. J., 1989, "Time Constants in Thermal

Laser Medicine," Lasers Surg. Med., **9**, pp. 405–421.

[25] Vogel, A., and Birngruber, R., 1992, "Temperature Profiles in Human Retina and Choroid During Laser Coagulation With Different Wavelengths Ranging From 514 to 810 nm," Lasers and Light in Ophthalmology, **5**(1), pp. 9–16.

[26] Flower, R. W., 2002, "Optimizing Treatment of Choroidal Neovascularization Feeder Vessels Associated With Age-Related Macular Degeneration," Am. J. Ophthalmol., **134**, pp. 228–239.

[27] Liu, V. G., Cowan, T. M., Jeong, S. W., Jacques, S. L., Lemley, E. C., and Chen, W. R., 2002, "Selective Photothermal Interaction Using an 805 nm Diode Laser and Indocyanine Green in Gel Phantom and Chicken Breast Tissue," Lasers Med. Sci., **17**(4), pp. 272–279.

[28] Yamashita, Y., Sakai, T., Watanabe, K., Maekawa, T., and Shirakusa, T., 1999, "Dye-Enhanced Selective Laser Ablation for Surgical Mucosectomy," Surg. Laparosc. Endosc. Percutan. Tech., **9**(6), pp. 387–391.

[29] Welch, A. J., and Van Gemert, M. J. C., 1995, *Optical-Thermal Response of Laser-Irradiated Tissue*, Plenum, New York.

[30] Welch, A. J., Wissler, E. H., and Priebe, L. A., 1980, "Significance of Blood Flow in Calculations of Temperature in Laser Irradiated Tissue," IEEE Trans. Biomed. Eng., **BME-27**(3), pp. 164–166.

[31] Welch, A. J., and Polhamus, G. D., 1984, "Measurement and Prediction of Thermal Injury in the Retina of the Rhesus Monkey," IEEE Trans. Biomed. Eng., **31**, pp. 633–644.

[32] Welch, A. J., Pearce, J. A., Diller, K. R., Yoon, G., and Cheong, W. F., 1989, "Heat Generation in Laser Irradiated Tissue," J. Biomed. Eng., **111**, pp. 62–68.

[33] Hammer, M., Roggan, A., Schweitzer, A., and Muller, G., 1995, "Optical Properties of Ocular Fundus Tissues—An In Vitro Study Using the Double-Integrating-Sphere Technique and Inverse Monte Carlo Simulation," Phys. Med. Biol., **40**, pp. 963–978.

[34] Moritz, A. R., and Henriques, F. C., 1947, "The Relative Importance of Time and Surface Temperature in the Causation of Cutaneous Burns," Am. J. Pathol., **23**, pp. 695–720.

[35] Pfefer, T. J., Choi, B., Vargas, G., Mcnally, K. M., and Welch, A. J., 2000, "Pulsed Laser-Induced Thermal Damage in Whole Blood," ASME J. Biomech. Eng., **122**, pp. 196–202.

[36] Geeraets, W. J., and Berry, E. R., 1968, "Ocular Spectral Characteristics As Related to Hazards From Lasers and Other Light Sources," Am. J. Ophthalmol., **66**(1), pp. 15–20.

[37] Gopalakrishnan, P., Kazmierczak, J. M., and Banerjee, R. K., 2005, "Influence of Repetition Frequency on Selective Retinal Photocoagulation For Macular Diseases," *Proceedings of The Summer Bioengineering Conference*, Paper No. B0276293.

[38] Tompkins, D. T., Klein, S. A., and Steeves, R. A., 1997, "Temperature Distributions during Thermoradiotherapy: A Sensitivity Study With a Transient Numerical Model of the Rabbit Eye," ASME J. Biomech. Eng., **119**, pp. 153–158.

[39] Birngruber, R., Hillenkamp, F., and Gabel, V. P., 1985, "Theoretical Investigations of Laser Thermal Retinal Injury," Health Phys., **48**(6), pp. 781–796.

[40] Gerner, E. W., 1987, "Thermal Dose and Time-Temperature Factors for Biological Responses to Heat Shock," Int. J. Hyperthermia, **3**(4), pp. 319–327.

[41] Jia, W., Aguilar, G., Verkruysse, W., Franco, W., and Nelson, J. S., 2006, "Improvement of Port Wine Stain Laser Therapy by Skin Preheating Prior to Cryogen Spray Cooling: A Numerical Simulation," Lasers Surg. Med., **38**, pp. 155–162.

[42] Zhu, L., Zheng, Y., von Kerczek, C., Topoleski, L. T. D., and Flower, R. W., 2006, "Feasibility of Extracting Velocity Distribution in Choriocapillaris in Human Eyes from ICG Dye Angiograms," ASME J. Biomech. Eng., **128**(2), pp. 203–209.